EMBO reports

scientific report

Inter-subunit interaction and quaternary rearrangement defined by the central stalk of prokaryotic V_1-ATPase

Nobutaka Numoto[1†], Yu Hasegawa[1*], Kazuki Takeda[1] & Kunio Miki[1,2+]*

[1]Department of Chemistry, Graduate School of Science, Kyoto University, Sakyo-ku, Kyoto, Japan, and [2]RIKEN SPring-8 Center, Harima Institute, Sayo, Hyogo, Japan

V-type ATPases (V-ATPases) are categorized as rotary ATP synthase/ATPase complexes. The V-ATPases are distinct from F-ATPases in terms of their rotation scheme, architecture and subunit composition. However, there is no detailed structural information on V-ATPases despite the abundant biochemical and biophysical research. Here, we report a crystallographic study of V_1-ATPase, from *Thermus thermophilus*, which is a soluble component consisting of A, B, D and F subunits. The structure at 4.5 Å resolution reveals inter-subunit interactions and nucleotide binding. In particular, the structure of the central stalk composed of D and F subunits was shown to be characteristic of V_1-ATPases. Small conformational changes of respective subunits and significant rearrangement of the quaternary structure observed in the three AB pairs were related to the interaction with the straight central stalk. The rotation mechanism is discussed based on a structural comparison between V_1-ATPases and F_1-ATPases.

Keywords: V-ATPase; asymmetric; crystal structure; rotation; vacuolar type

EMBO reports (2009) **10**, 1228–1234. doi:10.1038/embor.2009.202

INTRODUCTION

V-type ATPases (V-ATPases) couple the transfer of protons or sodium ions across the membrane with ATP hydrolysis or synthesis through a rotary catalytic mechanism (Yoshida *et al*, 2001; Forgac, 2007). V-ATPases occur in the membranes of acidic organelles, such as lysosomes and endosomes in eukaryotic cells, maintaining acidic pH by pumping protons coupled with ATP hydrolysis. V-ATPases are also found in the plasma membranes of archaea and some eubacteria (Yokoyama *et al*, 1990). These prokaryotic V-ATPases and closely related A-ATPases (Grüber & Marshansky, 2008) are primarily responsible for ATP synthesis, which is the reverse of the ATP-driven proton pumping reaction.

V-ATPases are thought to originate from an ancestral enzyme in common with F-ATPases (Mulkidjanian *et al*, 2007), because they have similar structural and functional features (Noji *et al*, 1997; Imamura *et al*, 2003). Both enzymes consist of water-soluble components (V_1-ATPases and F_1-ATPases, respectively), catalyse ATP hydrolysis and synthesis, and contain membrane-embedded components (V_o and F_o, respectively) involved in proton and ion pumping. These two components are linked through a central stalk (a rotor) and peripheral stalks (stators).

The V-ATPase of the thermophilic eubacterium, *Thermus thermophilus*, synthesizes ATP (Yokoyama *et al*, 1998), whereas isolated soluble V_1-ATPase has been shown to exert ATP hydrolysis activity, as in the case of F_1-ATPase. The subunit compositions for V_1-ATPases and F_1-ATPases are A_3B_3DF and $\alpha_3\beta_3\gamma\delta\varepsilon$, respectively (Yokoyama *et al*, 2000, 2003; Yoshida *et al*, 2001; Imamura *et al*, 2003). Despite the similar structural compositions of V_1-ATPases and F_1-ATPases, detailed analyses of the rotation kinetics have revealed divergence in the torque and rotation steps. The estimated torque of F_1-ATPase is about 46 pN nm (Yasuda *et al*, 1998; Imamura *et al*, 2005), whereas that of V_1-ATPase is approximately 35 pN nm (Hirata *et al*, 2003; Imamura *et al*, 2005). The rotation proceeds in 120° steps in F_1-ATPase, and the 120° rotation can be separated into 80° and 40° sub-steps during hydrolysis of one molecule of ATP (Shimabukuro *et al*, 2003). By contrast, V_1-ATPase shows 120° rotation without sub-steps (Imamura *et al*, 2005). These observations suggest strongly that V_1-ATPases and F_1-ATPases utilize different rotation mechanisms due to the different subunit interactions, structural transitions and torque generation mechanism.

Crystal structures of A and B subunits of A-ATPase (Maegawa *et al*, 2006; Schäfer *et al* 2006; Kumar *et al*, 2008), and the F subunit of V-ATPase (Makyio *et al*, 2005) have been determined in their isolated states. However, structural information for the D subunit (homologous to the γ-subunit of F_1-ATPase) is still unclear. Electron microscopic studies at about 20 Å resolution

[1]Department of Chemistry, Graduate School of Science, Kyoto University, Sakyo-ku, Kyoto 606-8502, Japan
[2]RIKEN SPring-8 Center, Harima Institute, Koto 1-1-1, Sayo, Hyogo 679-5148, Japan
*These authors contributed equally to this work
[†]Present address: School of Natural System, College of Science and Engineering, Kanazawa University, Kanazawa, Ishikawa 920-1192, Japan
[+]Corresponding author. Tel: +81 75 753 4029; Fax: +81 75 753 4032;
E-mail: miki@kuchem.kyoto-u.ac.jp

Received 20 April 2009; revised 4 August 2009; accepted 4 August 2009; published online 25 September 2009

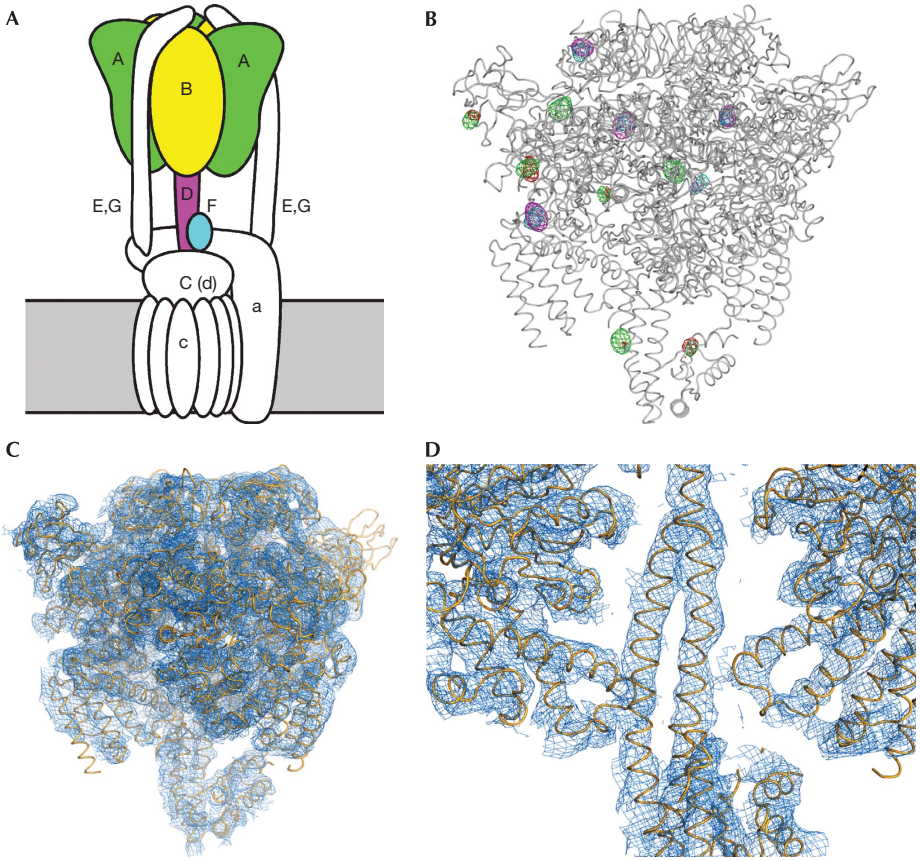

Fig 1 | Crystal structure of V_1-ATPase from *Thermus thermophilus*. (**A**) Schematic representation of the subunit composition of V-ATPase. The plasma membrane is indicated as a grey band. V_1-ATPase subunits are coloured. (**B**) Peaks on isomorphous and anomalous Fourier maps for a platinum derivative are shown as green and red meshes, whereas those for a mercury derivative are shown in purple and cyan. (**C**) An electron density map after phase combination is shown at the 1.2σ level. Electron density at one of the insertion domains of the A subunits (upper left of the molecule) is clearly observed. By contrast, corresponding electron densities at the other two domains are very weak (~0.5σ level; upper right and back side of the molecule), probably due to the lack of crystal contact. Therefore, the models for these two domains were built according to the model for the well-defined domain, and drawn as a half-transparent description. (**D**) Close-up view of the contact regions between the carboxy-terminal domain of the A and B subunits and the D subunit.

have provided only limited information about the subunit interactions (Bernal & Stock, 2004; Zhang *et al*, 2008). As the asymmetrical interaction between the central stalk and cylindrical A_3B_3 hexamer is thought to be of primary importance in the rotation mechanism, as in the case of F_1-ATPase (Yoshida *et al*, 2001; Kabaleeswaran *et al*, 2009), the detailed structure of the whole V_1-ATPase complex is indispensable for understanding the rotation mechanism.

Here, we report the crystal structure of V_1-ATPase from *T. thermophilus*. The rotation mechanism is discussed based on the interactions between subunits, and several meaningful differences have been observed between V_1-ATPases and F_1-ATPases in this regard.

RESULTS AND DISCUSSION

Structure determination

Intact V_1-ATPase (Fig 1A) was crystallized in nucleotide-free and nucleotide-bound forms. For the nucleotide-bound form, crystals were obtained by co-crystallization with Mg^{2+} ADP and aluminium fluoride (AlF_x). The structures were determined by using a combination of molecular replacement and multiple isomorphous replacement with anomalous scattering methods (Fig 1B; supplementary Table S1 online). The nucleotide-free structure was built as poly-alanine models and finally refined at 4.8 Å resolutions. For the D subunit, simulated annealing with a tight secondary structure restraint was carried out to fit the models of long helices into the electron density. Refinements were carried out by using rigid body refinement with several rigid domain definitions in each subunit (supplementary information online), and B-factor refinement using the same domain definitions. Two molecules of V_1-ATPases are contained in the asymmetric unit, and the final correlation coefficient of 0.920, for non-crystallographic symmetry averaging, indicates that these two complexes take almost the same conformation. The model of the nucleotide-bound form was built from the nucleotide-free structure and refined by using the same procedures as used for the nucleotide-free structure at 4.5 Å resolution (Fig 1C,D). The structures of these forms were almost the same, with an r.m.s.d. value of 0.44 Å for all Cα atoms (more than 3,266 atoms) in the superposition. Statistics are shown in Table 1.

Table 1 | Data collection, phasing and refinement statistics

	Nucleotide free	Nucleotide bound
Data collection		
Space group	*P*321	
Unit-cell parameters (Å)		
a	380.7	381.6
c	148.0	147.7
Resolutions (Å)	50–4.80 (4.97–4.80)	50–4.50 (4.66–4.50)
Number of observations	297,505	359,640
Number of unique reflections	57,305	70,598
Completeness (%)	95.2 (89.8)	96.9 (92.7)
Average $I/\sigma(I)$	13.4 (2.1)	10.3 (2.3)
Redundancy	5.2 (2.6)	5.1 (2.8)
R_{sym}* (%)	6.8 (37.5)	8.7 (41.7)
Phasing		
Combined figure of merit†	0.72	
NCS correlation coefficient	0.920	
Refinement		
Protein residues	6,532	6,532
ADP molecules	0	4
$R^{\ddagger}/R^{\S}_{free}$ (%)	44.1/45.2	43.0/43.6

Values in parentheses are for the highest resolution shell; *$R_{sym} = \sum\sum_i |I(h) - I(h)_i| / \sum\sum_i I(h)$, where $I(h)$ is the mean intensity; †Figure of merit is $\langle \cos(\Delta\alpha_h) \rangle$, where $\Delta\alpha_h$ is the error in the phase angle; ‡$R = \sum |F_o - F_c| / \sum |F_o|$, where F_o is the observed structure factor amplitude and F_c is the calculated structure factor amplitude; §R_{free} is as for R but calculated using a random set containing 5% of the data that were excluded during refinement.

Overall structure

V_1-ATPase has dimensions of approximately 120 Å (height) and 120 Å (diameter) at its maximum (Fig 2A,B). The central stalk composed of the D and F subunits protrudes about 40 Å from the A_3B_3 sub-assembly, similarly to that of F_1-ATPase consisting of γ-, δ- and ε-subunits. The most marked features of V_1-ATPase are attributed to the structure of the catalytic A subunit. An insertion domain between the amino-terminal β-barrel domain and nucleotide-binding domain is located outward from the spherical body of the A_3B_3 hexamer (Fig 2C). In addition, the carboxy-terminal helices of the A subunit also protrude. Owing to these protruding domains, the overall shape of the A_3B_3 hexamer is trapezoidal, with an increase of 20 Å in the maximum diameter compared with that of F_1-ATPase.

The A_3B_3 hexamer is assembled asymmetrically around a central stalk. Superposition (Fig 3A) and comparison of buried surface areas (supplementary Table S2 online) of three AB pairs with three αβ pairs clearly indicate that the A_WB_W pair forms a wide-open conformation. This also features in an $\alpha_E\beta_E$ pair, in which the active site is located at the interface region. By contrast, the A_NB_N and $A_{N'}B_{N'}$ pairs form a narrowly closed conformation, as do the $\alpha_{TP}\beta_{TP}$ and $\alpha_{DP}\beta_{DP}$ pairs. The A_WB_W pair can be superposed with a significantly lower r.m.s.d. value on the $\alpha_E\beta_E$ pair than on the $\alpha_{TP}\beta_{TP}$ or $\alpha_{DP}\beta_{DP}$ pair of bovine F_1-ATPase (supplementary Table S3 online). Consequently, A_NB_N and $A_{N'}B_{N'}$ pairs correspond to $\alpha_{TP}\beta_{TP}$ and $\alpha_{DP}\beta_{DP}$ pairs with the lowest r.m.s.d. values, respectively. We use the notations of the A and B subunits based on the quaternary state of each AB pair in this paper.

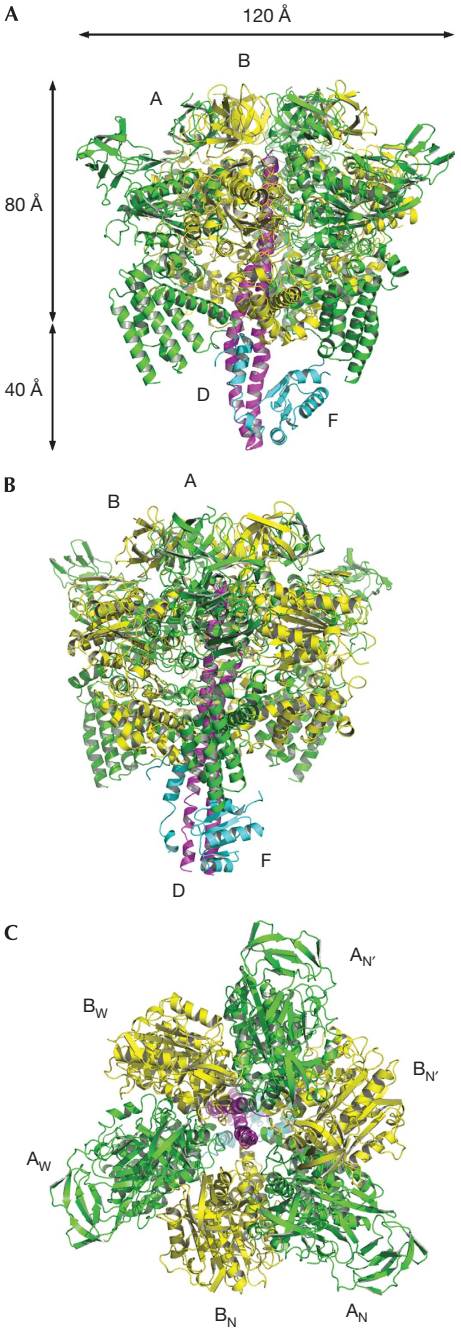

Fig 2 | Ribbon diagrams of V_1-ATPase. (**A**) A side view of V_1-ATPase. The A, B, D and F subunits are shown in green, yellow, purple and cyan, respectively. Approximate dimensions are indicated. (**B**) V_1-ATPase shown in (**A**) is rotated by about 60° around the perpendicular axis. (**C**) A top view looking towards the membrane of V_1-ATPase. All panels show the nucleotide-bound form.

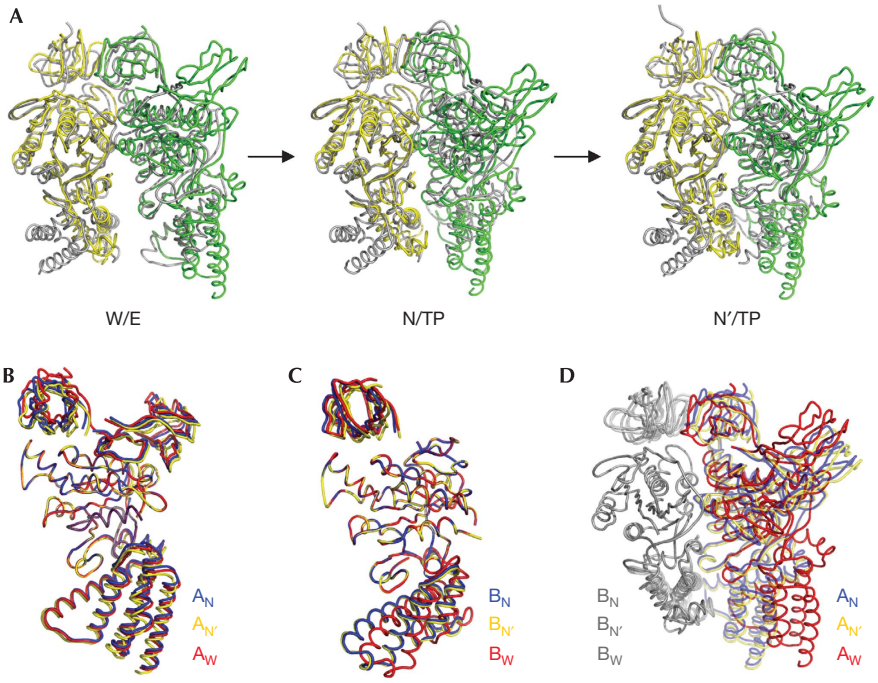

Fig 3 | Ternary and quaternary structure of A and B subunits. (**A**) A sequential view of rearrangement at the interface between A (in green) and B (in yellow) subunits. The α- and β-subunits of F_1-ATPase are shown in grey for comparison. Some incompatibility is observed between V_1-ATPase and F_1-ATPase in their carboxy-terminal domains, as additional helices are attached to the catalytic A subunit in V_1-ATPase and the non-catalytic α-subunit in F_1-ATPase. (**B**) A superposition of three catalytic A subunits. (**C**) A superposition of three non-catalytic B subunits. (**D**) A superposition of three AB pairs. The fit is carried out over B subunits.

The superposition of the three catalytic A subunits does not reveal the open–closed transition observed in the β-subunit of F_1-ATPase (Fig 3B). However, a superposition of three B subunits indicates that only the B_W subunit adopts the open conformation (Fig 3C). In contrast to the β-subunit of F_1-ATPase, however, the B_W subunit shows only small deviations from other B subunits.

Some significant differences are seen between the structures of A and B subunits in V_1-ATPase complex and the previously reported isolated structure. The N-terminal β-barrel domains of both subunits and the interface regions between the D subunit show primarily large deviations between complex and isolated structures (supplementary Fig S1 online). These facts indicate that sufficiently functional conformations of A and B subunits could be achieved only after the formation of the V_1 complex, or, at least, the A_3B_3 sub-complex.

Central stalk

Long coiled-coil helices of the D subunit are clearly seen in the electron density maps (Fig 4A; supplementary Fig S2 online). The lengths of the two helices are about 80 Å for the N-terminal helix (direction was determined in comparison with the structure and amino-acid sequence of the γ-subunit of F_1-ATPase) and 110 Å for the C-terminal helix. Superposition with the γ-subunit of bovine F_1-ATPase reveals the uncurved feature of these helices of V_1-ATPase (Fig 4A).

A significant electron density around the foot of the protruding region of the central stalk can be seen, and residues 1–75 of the structure of the F subunit (Makyio *et al*, 2005) are successfully placed in the electron density map (Fig 4B). The interpretation is validated using isomorphous/anomalous peaks (5.3 and 4.3σ at Met 1, and 7.3 and 3.1σ at Met 90 for the isomorphous and anomalous difference Fourier maps, respectively) from platinum derivative near the methionine residues. This region corresponds to the α/β-domain of the γ-subunit of F_1-ATPase. It is noteworthy that both the F subunit and α/β-domain of the γ-subunit show a Rossmann fold. However, the orientations differ from each other by about 90° (Fig 4C). The remaining density and another platinum peak near the N-terminal helix of the D subunit can be interpreted as the C-terminal helix (86–98) and Met 90 of the F subunit, respectively (Fig 4B). This conformation is not compatible with either the previously expected 'extended' or 'retracted' forms (supplementary Fig S3 online). However, our model for the F subunit is consistent for the cross-link experiments (Makyio *et al*, 2005) and reconstruction experiments (Imamura *et al*, 2004). Glu 8 of the F subunit is favourably located to be in contact with the C subunit, which is expected to be located between the central stalk of V_1-ATPase and the rotor ring of V_o (Iwata *et al*, 2004; Numoto *et al*, 2004), and Ala 75 is actually placed at the interface between the D subunit and the F subunit (Fig 2D). Moreover, the C-terminal helix has direct interactions with the C-terminal regions of A and B subunits (Fig 4D), by which the F subunit can modulate ATPase activity, as reported previously (Imamura *et al*, 2004).

There are some remaining densities around the coiled-coil helices of the D subunit (Fig 4D) that have not been interpreted. These densities might correspond to the non-helical middle region of the D subunit. Taking these densities into account, the overall diameter of the foot of the central stalk is estimated to be about

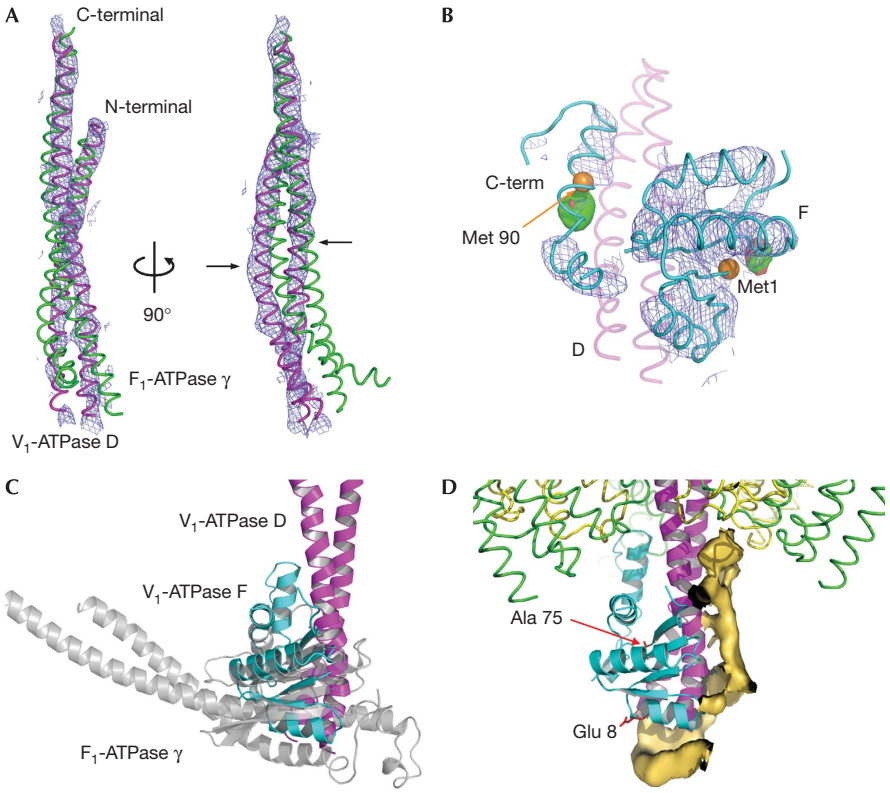

Fig 4 | Structure of the central stalk. (**A**) The coiled-coil helices of the D subunit (purple) are superposed with those of the γ-subunit of F_1-ATPase (green). Superposition was carried out by using the nucleotide-binding domains of the catalytic subunits between V_1-ATPase and F_1-ATPase (Gibbons *et al*, 2000). A blue mesh indicates the model-omitted electron density maps for the coiled-coil helices of the D subunit contoured at the 1.0σ level. Interface regions to the carboxy-terminal domain of the A and B subunits are indicated with black arrows. (**B**) An electron density around the F subunit in an omit map is shown as a blue mesh at the 1.0σ level. The F and D subunits are shown as cyan and purple tubes, respectively. Peaks on the isomorphous and anomalous difference Fourier map (contoured 4.0σ and 3.0σ level, respectively) of the platinum derivative are indicated as green and red surfaces. Cα atoms of the methionine residues are shown as orange spheres as a reference for the platinum-binding sites. (**C**) The D (purple) and F (cyan) subunits are superposed with the γ-subunit of F_1-ATPase (grey). The superposition was carried out by fitting the α/β-domain of the γ-subunit to the F subunit. (**D**) The foot portion of the central stalk. Residual electron densities (1.2σ level) around the stalk are represented as yellow surfaces. Side chains of Glu 8 and Ala 75 are represented as red sticks.

30 Å, which is significantly smaller than that of F_1-ATPase at about 50 Å. This smaller foot of the central stalk might be a feature of the interaction with the C subunit located between V_1-ATPase and V_o as an adaptor, as there is no counterpart for the C subunit in F-ATPases.

Nucleotide-binding sites

Significant peaks are seen in the difference ($F_{nucleotide}-F_{free}$) electron density map at the nucleotide-binding sites of the A subunits (Fig 5A). In A_N and $A_{N'}$ subunits, spheroidal peaks (6.8σ and 6.7σ, the two largest peaks in the molecule) are observed at the P loops (Fig 5B,C). The superposition of the β_{TP} and β_{DP} subunits of ADP–AlF_4^--bound F_1-ATPase (Menz *et al*, 2001) reveals that the phosphate groups fit well with the density map, strongly suggesting that this density corresponds primarily to the bound phosphate groups of ADP. Indeed, the phase-combined, density-modified map at the nucleotide binding sites indicates that no nucleotides are bound in the nucleotide-free form (supplementary Fig S4A,C online). By contrast, a similar map for the nucleotide-bound form reveals apparently protruding electron density thought to be bound nucleotide (supplementary Fig S4B,D online). Although AlF_x was included in the crystallization condition, at the present resolution it is difficult to evaluate whether bound nucleotides are ADP alone or ADP–AlF_x complexes. The negative peak near the N′ site corresponds to the residues of a helix following the P loop, so that this peak might be due to some conformational change of the helix upon nucleotide binding. In fact, the structure of the P loop region in the A subunit might be flexible because large conformational changes (supplementary Fig S1 online) are observed between V_1-ATPase and the isolated form (Maegawa *et al*, 2006).

However, only small positive and negative densities are seen in the difference map at the catalytic site of the A_W subunit (Fig 5D). Therefore, we interpret these results as indications that nucleotides are bound in the A_N and $A_{N'}$ subunits, whereas no nucleotide is bound in the A_W subunit. These properties of the electron density at the nucleotide-binding sites are consistent between two molecules in the asymmetric unit, except for their peak values.

Despite some evidence that the B subunit of V-ATPases binds to nucleotides (Schäfer & Meyering-Vos, 1992; Schäfer *et al* 2006;

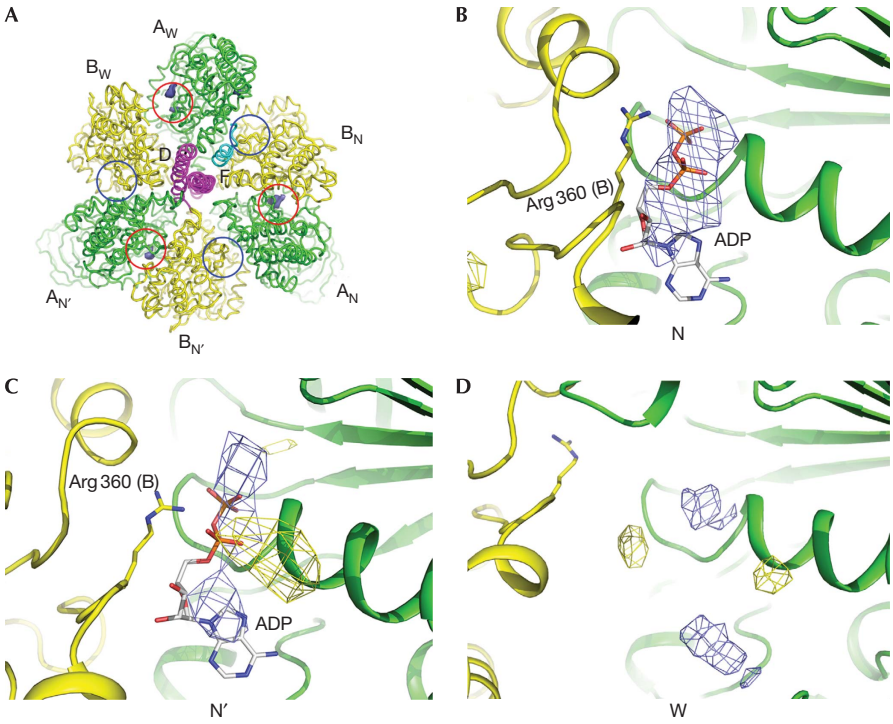

Fig 5 | Nucleotide-binding sites. (**A**) The bottom view of V_1-ATPase. The difference ($F_{nucleotide}-F_{free}$) map is shown as blue surfaces contoured at the $+5.0\sigma$ level. The catalytic sites of the A subunits are indicated by red circles and possible nucleotide-binding sites of B subunits are indicated by blue circles. (**B**) The subunit interface between A_N and B_N. The difference map is shown as blue and yellow meshes contoured at the $+5.0\sigma$ and -4.0σ levels, respectively. The side chain of Arg 360 and the model of ADP are drawn by the superposition of the structure of the F_1-ATPase (Menz *et al*, 2001). (**C**) The subunit interface between $A_{N'}$ and $B_{N'}$. (**D**) The subunit interface between A_W and B_W.

Kumar *et al*, 2008), there are no densities found in any of the non-catalytic B subunits (Fig 3A), indicating that no nucleotides are bound in the B subunits under our crystallization conditions.

Rotation mechanism of V-type ATPase

The active site of V_1-ATPase consists not only of residues of the A subunit but also of Arg360 of the B subunit, which is conserved between V_1-ATPases and F_1-ATPases (Fig 5B–D). The ternary and quaternary structure of each AB pair in V_1-ATPase is almost identical in the nucleotide-free and nucleotide-bound forms. Recently, it has been reported that the nucleotide-free structure of yeast F_1-ATPase forms an asymmetric structure quite close to that of nucleotide-bound enzyme (Kabaleeswaran *et al*, 2009). However, the structure of the nucleotide-free $\alpha_3\beta_3$ sub-complex of bacterial F_1-ATPase, lacking the central stalk, reveals an almost completely threefold symmetric feature (Shirakihara *et al*, 1997). These facts imply that asymmetric interactions between the A_3B_3 hexamer and the central stalk are primarily responsible for the formation of the asymmetric quaternary structure of the AB pairs. As the quaternary arrangement of the three asymmetric AB pairs and $\alpha\beta$ pairs are quite similar among V_1-ATPase, bovine and yeast F_1-ATPases from completely different crystal packing, these structures are unlikely to be the crystalline artefacts.

There are no significant open–closed transitions in the catalytic A subunits of V_1-ATPase, although the large ternary structural change of the catalytic β-subunit, especially the open–closed transition of the C-terminal helical region, is responsible for the torque generation in F_1-ATPase. Little rotation of the central stalk was observed between V_1-ATPase and F_1-ATPase when both structures are superposed. Therefore, it is plausible that the linear feature of the coiled-coil helices of the D subunit causes small ternary changes at A and B subunits. Thus, the torque is primarily generated by quaternary rearrangement at the interface between A and B subunits rather than the open–closed transition of the catalytic A subunit (supplementary Fig S5 online).

Speculation

The asymmetric quaternary structure of the three AB pairs and the $\alpha_3\beta_3$ pairs are similar (Fig 3A). The main structural difference between V_1-ATPase and F_1-ATPase are the ternary changes in the catalytic subunits, which are thought to have the crucial function of rotating the γ-subunit. A lack of these ternary changes at the catalytic A subunits might be an explanation for the relatively small torque of V_1-ATPase. These differences would provide the common essence of the rotary mechanism.

METHODS

Purification and crystallization. *T. thermophilus* HB8 was grown as reported previously by Yokoyama *et al* (1990). Cells were disrupted by sonication. Membranes were precipitated by centrifugation and suspended in 50 mM Tris–HCl (pH 8.0) and 1 mM EDTA. A total of 50 ml chloroform was added and the solution was vigorously stirred for 30 min. The supernatant containing solubilized V_1-ATPase was applied to columns of diethylaminoethyl-toyopearl

650S (TOSOH, Tokyo, Japan), Resource ISO (GE Healthcare, Uppsala, Sweden) and HiLoad 16/60 Superdex 200 (GE Healthcare). Protein was concentrated to 30 mg/ml in 10 mM Tris–HCl (pH 8.0) for crystallization experiments.

Crystals of V_1-ATPase were obtained in a 1:1 mixture of protein and reservoir solution containing 100 mM Na-2-(*N*-morpholino)ethanesulphonic acid (pH 6.0), 1.6 M $(NH_4)_2SO_4$, and 10% (v/v) dioxane, using the sitting-drop vapour-diffusion method at 20 °C. For the nucleotide-bound enzyme, a final concentration of 1 mM $Al(NO_3)_3$ and KF was added to the protein solution before crystallization. After 45 min, ADP and $MgCl_2$ were added to a final concentration of 10 mM. Heavy atom derivatives were prepared by soaking nucleotide-free crystals in solutions containing 5–10 mM of the heavy-atom compound of interest. Detailed information about protein purification and crystallization is described in the supplementary information online.

Structure solution and refinement. Before data collection, crystals were soaked in a cryoprotectant solution of 100 mM Na-2-(*N*-morpholino)ethanesulphonic acid. (pH 6.0), 1.9 M $(NH_4)_2SO_4$ and 20% (v/v) glycerol and flash-frozen under a nitrogen gas stream at −183 °C. X-ray diffraction experiments were carried out at beamlines BL17A in Photon Factory, and BL38B1, BL41XU and BL44XU in SPring-8. The structures were determined by a combination of molecular replacement and multiple isomorphous replacement with anomalous scattering methods. The models were built and refined as poly-alanine models (see main text). Further details about data processing, structure determination and statistics are described in the supplementary information online.

Coordinates. The structure of nucleotide-free and nucleotide-bound V_1-ATPases have been deposited in the Protein Data Bank (accession codes 3A5D and 3A5C).

Supplementary information is available at *EMBO reports* online (http://www.emboreports.org).

ACKNOWLEDGEMENTS

We thank the beamline staff at BL17A in Photon Factory, and BL38B1, BL41XU and BL44XU in SPring-8 for their help during the data collection. We also thank M. Yoshida, K. Yokoyama, T. Nogi and T.A. Fukami for their contribution in the early stages of the project. This study was supported by a grant (to KM) from the National Project on Protein Structural and Functional Analyses.

CONFLICT OF INTEREST

The authors declare that they have no conflict of interest.

REFERENCES

Bernal RA, Stock D (2004) Three-dimensional structure of the intact *Thermus thermophilus* H^+-ATPase/synthase by electron microscopy. *Structure* **12:** 1789–1798

Forgac M (2007) Vacuolar ATPases: rotary proton pumps in physiology and pathophysiology. *Nat Rev Mol Cell Biol* **8:** 917–929

Gibbons C, Montgomery MG, Leslie AG, Walker JE (2000) The structure of the central stalk in bovine F_1-ATPase at 2.4 Å resolution. *Nat Struct Biol* **7:** 1055–1061

Grüber G, Marshansky V (2008) New insights into structure-function relationships between archeal ATP synthase (A_1A_0) and vacuolar type ATPase (V_1V_0). *Bioessays* **30:** 1096–1109

Hirata T, Iwamoto-Kihara A, Sun-Wada GH, Okajima T, Wada Y, Futai M (2003) Subunit rotation of vacuolar-type proton pumping ATPase: relative rotation of the G and C subunits. *J Biol Chem* **278:** 23714–23719

Imamura H, Nakano M, Noji H, Muneyuki E, Ohkuma S, Yoshida M, Yokoyama K (2003) Evidence for rotation of V_1-ATPase. *Proc Natl Acad Sci USA* **100:** 2312–2315

Imamura H, Ikeda C, Yoshida M, Yokoyama K (2004) The F subunit of *Thermus thermophilus* V_1-ATPase promotes ATPase activity but is not necessary for rotation. *J Biol Chem* **279:** 18085–18090

Imamura H, Takeda M, Funamoto S, Shimabukuro K, Yoshida M, Yokoyama K (2005) Rotation scheme of V_1-motor is different from that of F_1-motor. *Proc Natl Acad Sci USA* **102:** 17929–17933

Iwata M *et al* (2004) Crystal structure of a central stalk subunit C and reversible association/dissociation of vacuole-type ATPase. *Proc Natl Acad Sci USA* **101:** 59–64

Kabaleeswaran V, Shen H, Symersky J, Walker JE, Leslie AGW, Mueller DM (2009) Asymmetric structure of the yeast F_1 ATPase in the absence of bound nucleotides. *J Biol Chem* **284:** 10546–10551

Kumar A, Manimekalai MS, Grüber G (2008) Structure of the nucleotide-binding subunit B of the energy producer A_1A_0 ATP synthase in complex with adenosine diphosphate. *Acta Crystallogr D Biol Crystallogr* **64:** 1110–1115

Maegawa Y, Morita H, Iyaguchi D, Yao M, Watanabe N, Tanaka I (2006) Structure of the catalytic nucleotide-binding subunit A of A-type ATP synthase from *Pyrococcus horikoshii* reveals a novel domain related to the peripheral stalk. *Acta Crystallogr D Biol Crystallogr* **62:** 483–488

Makyio H *et al* (2005) Structure of a central stalk subunit F of prokaryotic V-type ATPase/synthase from *Thermus thermophilus*. *EMBO J* **24:** 3974–3983

Menz RI, Walker JE, Leslie AG (2001) Structure of bovine mitochondrial F_1-ATPase with nucleotide bound to all three catalytic sites: implications for the mechanism of rotary catalysis. *Cell* **106:** 331–341

Mulkidjanian AY, Makarova KS, Galperin MY, Koonin EV (2007) Inventing the dynamo machine: the evolution of the F-type and V-type ATPases. *Nat Rev Microbiol* **5:** 892–899

Noji H, Yasuda R, Yoshida M, Kinosita K Jr (1997) Direct observation of the rotation of F_1-ATPase. *Nature* **386:** 299–302

Numoto N, Kita A, Miki K (2004) Structure of the C subunit of V-type ATPase from *Thermus thermophilus* at 1.85 Å resolution. *Acta Crystallogr D Biol Crystallogr* **60:** 810–815

Schäfer G, Meyering-Vos M (1992) F-type or V-type? The chimeric nature of the archaebacterial ATP synthase. *Biochim Biophys Acta* **1101:** 232–235

Schäfer IB, Bailer SM, Düser MG, Börsch M, Bernal RA, Stock D, Grüber G (2006) Crystal structure of the archaeal A_1A_o ATP synthase subunit B from *Methanosarcina mazei* Gö1: Implications of nucleotide-binding differences in the major A_1A_o subunits A and B. *J Mol Biol* **358:** 725–740

Shimabukuro K, Yasuda R, Muneyuki E, Hara KY, Kinosita K Jr, Yoshida M (2003) Catalysis and rotation of F_1 motor: cleavage of ATP at the catalytic site occurs in 1 ms before 40 degree substep rotation. *Proc Natl Acad Sci USA* **100:** 14731–14736

Shirakihara Y *et al* (1997) The crystal structure of the nucleotide-free $\alpha_3\beta_3$ subcomplex of F_1-ATPase from the thermophilic *Bacillus* PS3 is a symmetric trimer. *Structure* **5:** 825–836

Yasuda R, Noji H, Kinosita K Jr, Yoshida M (1998) F_1-ATPase is a highly efficient molecular motor that rotates with discrete 120 degree steps. *Cell* **93:** 1117–1124

Yokoyama K, Oshima T, Yoshida M (1990) *Thermus thermophilus* membrane-associated ATPase. Indication of a eubacterial V-type ATPase. *J Biol Chem* **265:** 21946–21950

Yokoyama K, Muneyuki E, Amano T, Mizutani S, Yoshida M, Ishida M, Ohkuma S (1998) V-ATPase of *Thermus thermophilus* is inactivated during ATP hydrolysis but can synthesize ATP. *J Biol Chem* **273:** 20504–20510

Yokoyama K, Ohkuma S, Taguchi H, Yasunaga T, Wakabayashi T, Yoshida M (2000) V-Type H^+-ATPase/synthase from a thermophilic eubacterium, *Thermus thermophilus*. Subunit structure and operon. *J Biol Chem* **275:** 13955–13961

Yokoyama K, Nagata K, Imamura H, Ohkuma S, Yoshida M, Tamakoshi M (2003) Subunit arrangement in V-ATPase from *Thermus thermophilus*. *J Biol Chem* **278:** 42686–42691

Yoshida M, Muneyuki E, Hisabori T (2001) ATP synthase—a marvellous rotary engine of the cell. *Nat Rev Mol Cell Biol* **2:** 669–677

Zhang Z, Zheng Y, Mazon H, Milgrom E, Kitagawa N, Kish-Trier E, Heck AJ, Kane PM, Wilkens S (2008) Structure of the yeast vacuolar ATPase. *J Biol Chem* **283:** 35983–35995